Polarization-Shaped Strong Field Control Over Valley Polarization with Mid-IR Light

Igor Tyulnev, Julita Poborska, Álvaro Jiménez-Galán, Lenard Vamos, Olga Smirnova, Mikhail Ivanov, and Jens Biegert

Abstract We induce valley-control in MoS_2 with a polarization-shaped mid-infrared light field. The trefoil-shaped pump field is characterized by high harmonic spectroscopy and valley polarization is read our by a probe field via second harmonic generation.

Keywords Valleytronics · TMDC · Two-dimensional · High-harmonic generation · High-harmonic spectroscopy · Strong-field · Sub-cycle · Lightwave electronics · Optical control

I. Tyulnev · J. Poborska · L. Vamos
ICFO – Institut de Ciencies Fotoniques, The Barcelona Institute of Science and Technology, Barcelona, Spain

Á. Jiménez-Galán
Max-Born-Institut, Berlin, Germany

O. Smirnova
Max-Born-Institut, Berlin, Germany

Technische Universität Berlin, Berlin, Germany

M. Ivanov
Max-Born-Institut, Berlin, Germany

Institute für Physik, Humboldt-Universität zu Berlin, Berlin, Germany

Department of Physics, Imperial College London, London, UK

J. Biegert (✉)
ICFO – Institut de Ciencies Fotoniques, The Barcelona Institute of Science and Technology, Barcelona, Spain

ICREA, Barcelona, Spain
e-mail: jens.biegert@icfo.eu

L. Argenti et al. (eds.), *Proceedings of the 8th International Conference on Attosecond Science and Technology*, Springer Proceedings in Physics 300,
https://doi.org/10.1007/978-3-031-47938-0_19

1 Introduction

Polarization shaping of the temporal evolution of an optical light field provides additional degrees of freedom to interrogate matter and control its properties. The emergent complex electrical currents are controlled on the sub-cycle scale of the optical field and provide enticing new ways to process information or to switch the properties of a material on ultrafast timescales. The non-linear motion of field-driven electrons in a material radiate at optical frequencies; thus, detecting high-order harmonic radiation provides insight into the dynamic evolution of carriers. This potential was first recognized in Ref. [1] with the detection of high harmonics (HH) of the mid-IR driver in bulk ZnO and led to numerous investigations of the electron-hole dynamics [2, 3], of many-body effects in correlated systems [4], the interplay of different bands [5], and recently the detection of quantum phases in superconductors [6]. Confining the dynamics to two-dimensional layers, e.g., in graphene-like materials or transition-metal-dichalcogenides (TMDCs), allows for the study of HH dynamics below and above the bandgap without complicating the interpretation due to propagation effects [7]. The broken inversion symmetry of a monolayer led to observation of Berry curvature dependent effects [8]. Rotation of the light's polarization vector determines the recombination times of electron-hole trajectories from K and K′ symmetry points [7]. In contrast, circular polarization carries spin angular momentum that lifts the valley degeneracy through optical selection rules [9, 10].

Here, we extend the control over the valley degree of freedom into the strong-field regime by matching the driving field polarization to the crystal symmetry of 2H-MoS2. To this end, we shape the polarization of the optical electric field into a three-fold symmetric "trefoil" shape. To achieve such three-fold symmetry, we combine pulses of two colors while manipulating the handedness of their circular polarization. The so-tailored field is characterized by symmetry-resolved chiral spectroscopy, where selection rules result in circularly polarized harmonics of odd and even orders from the inversion symmetric material. With the off-resonant strong-field trefoil acting as a pump, a modulation in the bandgap at high symmetry points K and K′ is observed in a non-collinear geometry pump-probe experiment.

The measurement of the second harmonic of the probe field is a clear sign of the valley polarization induced by the trefoil pump field.

2 Valley Polarization in MoS_2

The light carries spin angular momentum and can, thus, induce asymmetry of carriers between valleys in reciprocal space during resonant excitation of the bandgap in the K/K′ points. The degree of circular polarization is linked to the valley contrasting magnetic moment "m," which defines the coupling strength $|P|^2$. For the quantum number "m" to be non-zero, the spatial inversion symmetry of

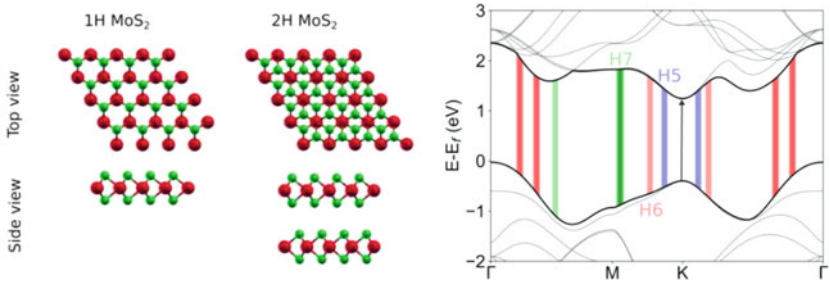

Fig. 1 Left: Top and side view of the trigonal prismatic crystal structure of 1H- and 2H-MoS_2. Right: 2H-MoS_2 band structure; Blue, red, and green represent gaps that fit H5, H6, and H7 emission energies and the bandwidth of the 3.2 μm driving field

the crystal must be broken. Such inversion symmetry breaking occurs naturally for monolayer TMDCs. The material becomes valley polarized, and the electron motion depends on the sign of the valley index and the Berry curvature at the respective high symmetry point [11].

In contrast, a bi-layer system in the 2H phase is symmetric under spatial inversion due to the rotated second layer (Fig. 1), and valley asymmetry cannot be induced with circularly polarized light. However, symmetry breaking can be re-introduced through the structuring of light when the system is excited off-resonantly by a trefoil-shaped strong field. In the following, we leverage this prospect for inducing valley polarization.

3 Polarization Shaping and Trefoil Generation

We use our home-built mid-infrared OPCPA system [12] at 3.2 μm for the experiment. For the polarization shaping, a 97 fs pulse is split within a Mach-Zehnder interferometer into two components in which one is frequency doubled. The polarization states and intensity ratio between fundamental and second harmonic are carefully controlled by waveplates. Both beams are recombined and then focused onto the sample. We use a vacuum electric field amplitude of 0.05 V/Å in the mid-IR and derive the probe beam at 800 nm from the same OPCPA with full optical synchronization. The pump-probe experiment is performed in non-collinear geometry to ensure the distinguishability of components from the trefoil pump and 800-nm probe.

4 Polarization Resolved Chiral Spectroscopy

First, we perform chiral spectroscopy to confirm the trefoil shape of the pump beam. Analog to Ref [13], we generate HHs in GaSe with varying polarization shapes of the driving field.

Figure 2 shows the results for the measurement of harmonic orders 5–7 (H5-H7). The figure shows how the harmonic signals vary with crystal rotation. Lineouts of H5 are also shown on a polar plot with the polarization type illustrated. The left column is the HH spectrum for a linearly polarized 3.2 μm driving field. The harmonic response from the hexagonal crystal yields six peaks during a full rotation scan. The harmonic intensity is maximized when the laser polarization aligns with the crystal axis which occurs every 60° and completely disappears with the polarization rotated 30° further. Changing the driving field to circular polarization minimizes the H6 signal due to optical selection rules [14], while the other harmonics do not show any clear angle dependence due to the isotropic polarization. Finally, the two-color trefoil field shows three-fold symmetry in the H5 and H7 responses, which show maxima 120° apart. This behavior is understood when considering the crystal as a combination of Ga and Se sublattices, which are addressed by the trefoil three times each in a full rotation. Having confirmed the generation of a trefoil field, we now turn to the TMDC.

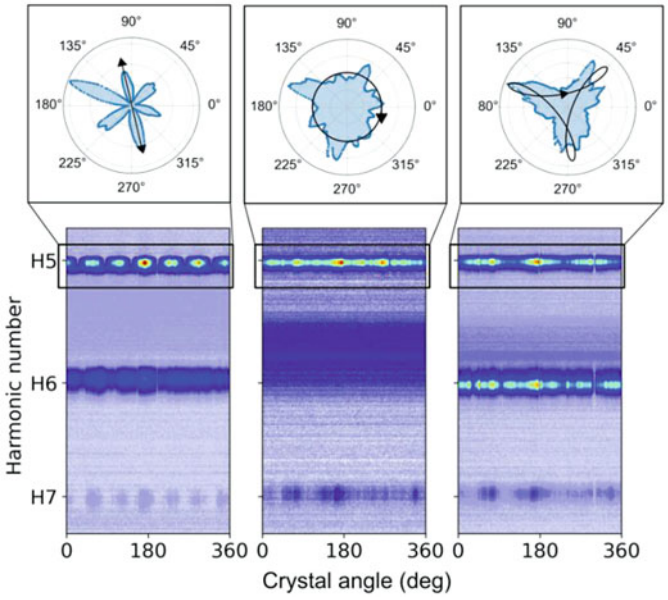

Fig. 2 Polarization scans for linear, circular, and trefoil driving fields. Harmonic spectra from GaSe are recorded as a function of the crystal rotation angle

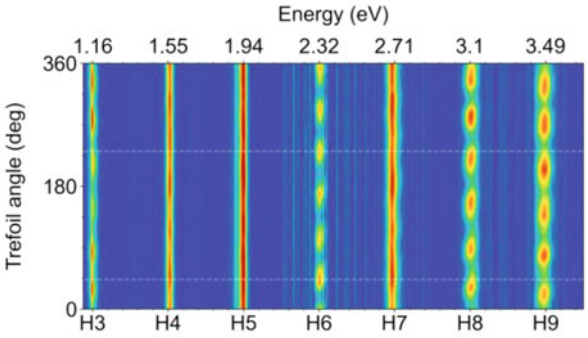

Fig. 3 The trefoil field drives high harmonic spectrum in 2H-MoS_2 as a function of the polarization rotation

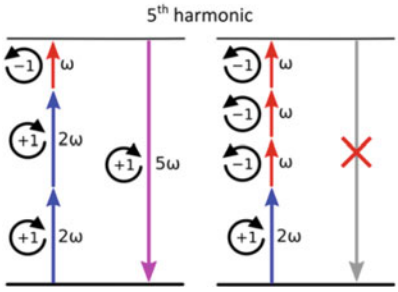

Fig. 4 Trefoil selection rules from two-color photon mixing with opposite spin-angular momentum

To investigate strong field-induced valley polarization, we used a 10-μm thin crystal of 2H-MoS_2. The material is mounted without substrate, thus avoiding contamination and background.

Figure 3 shows the recorded spectra for 360° of polarization rotation of the trefoil field only. Due to the six-fold symmetry of the material's 2H phase, we find that each harmonic modulates with 60° periodicity. This is in accord with scans in which the linear polarization aligns with the crystal axis. Note that 2H-MoS2's lowest band gap of 1.66 eV is at the K point, while the gaps at Γ and M are at 2.43 eV and 2.76 eV, respectively. From the transitions illustrated in Fig. 1, H5 is the first inter-band harmonic since it gets emitted closest to the K point.

As previously explained, although the sample is inversion symmetric, the bi-circular pump generates even harmonics. We also find that the strengths of H3 and H6 reduce by several orders of magnitude. This is explained by the selection rules (3 N + 1) and (3 N + 2) due to the conservation of spin-angular momentum during the frequency mixing of the two colors (see Fig. 4). Note that according to theory, harmonic orders (3 N) are forbidden. We attribute the observable small signal to slight imperfections of the pump, i.e., slight ellipticity of the pump polarization [15]. However, the strong and clear modulation of the signal with similar peak amplitudes over the 360° rotation proves the existence of a symmetric trefoil shape.

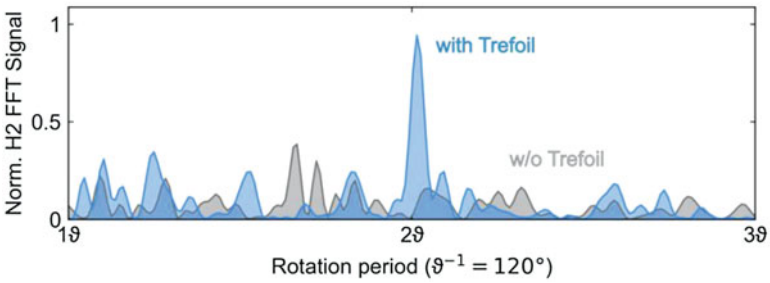

Fig. 5 Shown is the probe (H2) signal's dependency on the pump trefoil rotation. A clear modulation with 60° periodicity appears during strong field excitation, matching the six-fold symmetry of the 2H-MoS_2 sample

5 Strong Field-Induced Valley Control

Figure 5 shows the modulation of the second harmonic (SH) signal generated by the probe beam. A Fast Fourier Transform (FFT) of two different measurements, one with the trefoil as a pump and one without a trefoil, clearly shows that the trefoil field indeed induces non-resonant valley polarization.

When applying the trefoil field and rotating its polarization angle, the probe exhibits modulation every 60° of the pump's rotation; this shows in the FFT as a peak at 2 theta. As discussed in [16], strong-field interaction between the trefoil field and 2D materials like 1H-MoS2 reduces the band gap at the K or K′ points, depending on the orientation of the trefoil. Note that this process is not limited to the monolayer due to the off-resonant excitation and is, thus, universal.

6 Summary

We show experimental results from polarization-shaped trefoil fields that non-resonantly induce valley polarization in a TMDC material. Generating and measuring the effects of valley polarization are all-optical, thus providing control over material properties at the sub-cycle scale of PHz optical fields. High harmonic spectroscopy is employed to characterize and measure the efficacy of valley polarization.

Acknowledgments J.B. and group acknowledge financial support from the European Research Council for ERC Advanced Grant "TRANSFORMER" (788218), ERC Proof of Concept Grant "miniX" (840010), FET-OPEN "PETACom" (829153), FET-OPEN "OPTOlogic" (899794), FET-OPEN "TwistedNano" (101046424), Laserlab-Europe (871124), Marie Skłodowska-Curie ITN "smart-X" (860553), MINECO for Plan Nacional PID2020–112664 GB-I00; AGAUR for 2017 SGR 1639, MINECO for "Severo Ochoa" (CEX2019-000910-S), Fundació Cellex Barcelona, the

CERCA Programme/Generalitat de Catalunya, and the Alexander von Humboldt Foundation for the Friedrich Wilhelm Bessel Prize.

References

1. Ghimire, S., DiChiara, A., Sistrunk, E., et al.: Observation of high-order harmonic generation in bulk crystal. Nat. Phys. **7**, 138–141 (2011)
2. Parks, A.M., Ernotte, G., Thorpe, A., McDonald, C.R., Corkum, P.B., Taucer, M., Brabec, T.: Wannier quasi-classical approach to high harmonic generation in semiconductors. Optica. **7**, 1764–1772 (2020)
3. Vampa, G., Hammond, T., Thiré, N., et al.: Linking high harmonics from gases and solids. Nature. **522**, 462–464 (2015)
4. Silva, R., Blinov, I., Rubtsov, A., Smirnova, O., Ivanov, M.: High harmonic imaging of ultrafast many-body dynamics in strongly correlated systems. Nat. Photo. **12**, 266 (2018)
5. Tancogne-Dejean, N., Mücke, O., Kärtner, F., Rubio, A.: Ellipticity dependence of high-harmonic generation in solids originating from coupled intraband and interband dynamics. Nat. Commun. **8**, 745 (2017)
6. Elu, U., et al.: High harmonic spectroscopy of quantum phase transitions in high-T_c superconductor. Proc. Natl. Acad. Sci. **119**(40), e2207766119 (2022)
7. Yoshikawa, N., Nagai, K., Uchida, K., et al.: Interband resonant high-harmonic generation by valley polarized electron–hole pairs. Nat. Commun. **10**, 3709 (2019)
8. Liu, H., Li, Y., You, Y., et al.: High-harmonic generation from an atomically thin semiconductor. Nat. Phys. **13**, 262–265 (2017)
9. Zeng, H., Dai, J., Yao, W., et al.: Valley polarization in MoS_2 monolayers by optical pumping. Nat. Nanotech. **7**, 490–493 (2012)
10. Liu, Y., Gao, Y., Zhang, S., et al.: Valleytronics in transition metal dichalcogenides materials. Nano Res. **12**, 2695–2711 (2019)
11. Xiao, D., Yao, W., Niu, Q.: Valley-contrasting physics in graphene: magnetic moment and topological transport. Phys. Rev. Lett. **99**, 23 (2007)
12. Elu, U., Maidment, L., Vamos, L., Biegert, J., et al.: Seven-octave high-brightness and carrier-envelope-phase-stable light source. Nat. Photonics. **15**, 277–280 (2021)
13. Heinrich, T., Taucer, M., Kfir, O., et al.: Chiral high-harmonic generation and spectroscopy on solid surfaces using polarization-tailored strong fields. Nat. Commun. **12**, 3723 (2021)
14. Nariyuki, S., Peiyu, X., Faming, L., Teruto, K., Jiro, I., Nobuhisa, I.: Observation of selection rules for circularly polarized fields in high-harmonic generation from a crystalline solid. Optica. **4**, 1333–1336 (2017)
15. Jiménez-Galán, Á., Zhavoronkov, N., Schloz, M., Morales, F., Ivanov, M.: Time-resolved high harmonic spectroscopy of dynamical symmetry breaking in bi-circular laser fields: the role of Rydberg states. Opt. Express. **25**, 22880–22896 (2017)
16. Jiménez-Galán, Á., Silva, R., Smirnova, O., et al.: Lightwave control of topological properties in 2D materials for sub-cycle and non-resonant valley manipulation. Nat. Photonics. **14**, 728–732 (2020)